SciEn
Journal of Engineering Advancements Vol. 03(03) 2022, pp 91-95 https://doi.org/10.38032/jea.2022.03.003

Characteristics of Ion Beam for Various Gases in a Spherical Plasma Focus Device

*M A Malek**

Physics Discipline, Khulna University, Khulna-9208, Bangladesh

Received: August 28, 2022, Revised: September 17, 2022, Accepted: September 18, 2022, Available Online: September 24, 2022

ABSTRACT

This study presents the computed ion beam properties (flux, fluence, and energy) of argon, neon, and nitrogen gases with pressure variation in the spherical plasma focus device, KPU200 SPF. Numerical experiments are performed using the Lee code (version: RADPFV5.16FIB) with the gases in the pressure range of 0.10 - 19 Torr. The electrode geometry has been obtained by applying the 'equivalent straightened electrode' technique. The computed results for each of the gases show that the ion beam properties increase with the increase in pressure until reach a peak value and then start to reduce with further pressure increase. The peak ion beam flux (ions m^{-2} s^{-1}), fluence (ions.m^{-2}), and energy (J) from heavier argon pinch plasma are found as 5.31×10^{27} at 2 Torr, 8.93×10^{20} at 3.5 Torr, and 3.46×10^{4} at 3 Torr, respectively which are the utmost values from neon and nitrogen gases. Significant correlations of pinch radius and duration, effective charge number, and induced voltage with these ion beam properties are noticed and discussed in this paper. The obtained results of this study are compared with those of the NX2 plasma focus device that makes the consistency of the present research work.

Keywords: Spherical Plasma Focus, Lee Code, Plasma Pinch, Ion Beam, Flux, Fluence.

1 Introduction

A dense plasma focus (DPF) device produces super-dense (~1016 - 1019 cm^{-3}), super-hot (~1 keV) plasma by self-generated electromagnetic compression [1]. It is a non-radioactive powerful source of ion beam (~0.01 - 100 MeV), electron beam (~0.01 - 1 MeV), pulsed fusion neutron (~2.45 - 14 MeV), soft (0.1 - 10 keV), and hard (~10 - 1000 keV) X-rays [2]-[3]. The first models of DPF are invented in the 1960s by Mather in the USA [4] and Filippov in USSR [5]-[6]. The operation principles of these two types are the same but differ in the aspect ratio (ratio of anode length to its radius) of their electrode geometry. A spherical plasma focus (SPF) having two concentric spherical electrodes (anode and cathode) is a special combination of the Mather and Filippov type of device.

A plasma focus is enclosed within a chamber, consisting of two co-axial electrodes separated by an insulator, powered by a high voltage capacitor bank. The filling gas starts to discharge across the electrodes due to the breakdown voltage and produces a plasma sheath (PS) over the surface of the insulator. This PS is then liftoff and accelerated by the axial Lorentz force (LF) across the coaxial electrodes. When it reaches at anode end, the radial LF pushes the PS towards the anode top forming a high-temperature, high-dense, very thin, and small shape plasma column known as pinch. This dense and hot plasma into the pinch column during its stagnation in front of the anode top is the source of radiation. Finally, it is collapsed by un-stabilities forming the voltage works to accelerate the electron and ion beam in opposite directions. The emitted high-energy ion and electron beams from pinch plasma in a DPF have been used in different fields such as nano-material and device fabrication [7], thin film deposition [8], surface modification [9], thermal surface treatment [10], ion-assisted coating [11], ion implication, and production of short-lived radioisotopes [12] including plasma processing. Many efforts have been made in experimental studies of applications of fast ion and electron beams from various DPF devices [13]. Most of the experiments in ion beam detection were performed with deuterium to investigate neutron production and deuteron acceleration during plasma focus discharge. The energy transfer mechanism from magnetized plasma to ions and electrons is unclear till today [14]. Therefore, ion beam characterization is not only very important for understanding the production mechanism of high-energy ions but also plays an important role in optimizing, upgrading, and modifying DPF devices for their specific application in different fields [15]-[17].

The Lee code [18]-[20] is one of the famous tools for numerical modeling and experiments [21] of a plasma focus for computing ion beam properties (flux, fluence, density, and energy) [22]-[23]. Ion beam characteristics have been studied in Mather and Flippov type devices using this code. The KPU200 is a spherical plasma focus device which is designed mainly for neutron production [24]-[25]. The electrode (anode & cathode) geometry, static inductance, operating voltage, and pressure change of different gases were studied for neutron and ion production [26]-[27], X-ray emissions (continuum and line radiations) [28]-[30] in this device. So far, no one has computed ion beam properties in this device.

In this paper, I study some characteristics such as peak discharge current (I_{peak}), pinch current (I_{pinch}) and radius (r_p), effective charge number, ion accelerating induced voltage taken as diode voltage which are directly used to calculate ion beam properties with pressure change in various gases including nitrogen (N_2), neon (Ne), and argon (Ar) from the spherical plasma focus device KPU200 SPF using the Lee code.

In section 2, I present a brief description of the operation including the calculating equations of ion beam flux, fluence, and energy in the Lee code, and the method of numerical experiments is given in section 3. In section 4, the results and discussions are presented and finally, conclusions are given in section 4.

2 The Lee Code

Around all of the main phases of discharge in a DPF can be simulated using the five-phase Lee code [31]. The plasma focus

*Corresponding Author Email Address: malek@ku.ac.bd Published by: SciEn Publishing Group

dynamics, thermodynamics, and radiations are coupled with the electrical circuit by this code. The effects of gas ionization, discharge by shock-wave heating in radial phase just before the formation of stable pinch, plasma heating in pinch column due to the ohmic for Spitzer and anomalous resistivity, and micro-instability development are included in the code. It shows the consistency of mass, energy, charge, and momentum. This code can be used in the experimental interpretation and design of a plasma focus [1]. It couples the radiations (bremsstrahlung, line, and recombination) with the dynamics of plasma pinch compression. In the code, the transition from volumetric to surface emission, self-absorption in plasma, fusion neutron production by beam-target as well as thermonuclear methods are also considered.

The discharge current waveform getting from a DPF operation can be considered a significant indicator of realistic simulation and analyze all of the gross properties of a plasma focus. Using the Lee code, the important information (axial and radial phase dynamics and radiations) of a device can be traced quickly from the current flow through the plasma sheath [19]. However, when the computed discharge current waveform is fitted with the measured one, the computed outputs of the code provide the following realistic data: the dynamics and energy in each phase, the geometry of pinch column, densities and temperatures, radiations, neutron yields, and ion beam.

Therefore, to simulate a specific DPF device by this code, the measured discharge current waveform of the device is to be picked out either from the published article or from a laboratory experiment.

2.1 The Ion Beam Flux, Fluence, and Energy Equations

To study the properties of the emitted ion beam from the pinch plasma in a DPF, the ion beam flux equation has been derived and inserted into the Lee code [19], [32]-[33]. At the time of simulation, the flux of the ion beam is estimated in the code with the following equation [22]:

$$Flux\ (ions\ m^{-2}\ s^{-1}) = 2.75 \times 10^{15} \left(\frac{f_e}{\sqrt{MZ_{eff}}}\right)\left(\frac{ln[b/r_p]}{r_p^2}\right)\frac{I_{pinch}^2}{\sqrt{U}} \quad (1)$$

Here, f_e is the fraction of pinch inductive energy (PIE) converted into the beam kinetic energy (BKE) and it is equivalent to an ion beam energy of (3 - 6) % E_0 (operating energy of plasma focus). To study the pinch dimensional-temporal relationships and the neutron yield data [22]-[23], the value of f_e has been estimated as 0.14 [23], M is the ion mass number, Z_{eff} is the number of effective charge of ion in the pinch, b is the cathode radius, the pinch radius, the pinch current are to be known. The ion accelerating voltage is taken as diode voltage U = $3V_{max}$, which is obtained from data fitting, where V_{max} is the maximum induced voltage of the pre-pinch radial phase. For the case of strong radiative collapse, it generates an additional induced voltage and, in such cases, U = V_{max}^* [22]-[23].

The ion fluence is defined as the number of ions per unit cross-section of the pinch column. Since the beam emits from the focus pinch with slight divergence, fluence is the best way to characterize the ion beam. It is calculated as the flux multiplied by the pulse duration of the ion beam (τ). From considering approximate scaling [23]: $\tau = 10^{-6} z_p$ where, z_p is the pinch column length. Thus:

$$Fluenc\ (ions\ m^{-2}) = 2.75 \times 10^9 \left(\frac{f_e}{\sqrt{MZ_{eff}}}\right)\left(\frac{ln[b/r_p]}{r_p^2}\right) \quad (2)$$

Ion beam energy (E) is estimated by using the following equation:

$$E(J) = Z_{eff} U \times Number\ of\ ion\ in\ beam \quad (3)$$

The code computes the values of Z_{eff}, r_p, pinch duration, I_{pinch}, and U along with the ion beam flux followed by ion beam fluence and energy.

3 Method used in Numerical Experiments

In this work, I use the Spherical Plasma Focus, KPU200 SPF for the numerical studies of the ion beam flux, fluence, and energy in various gases including N_2, Ne, and Ar with pressure variation. The electrode geometry has been obtained by applying the 'equivalent straightened electrode' technique to this SPF device [24]-[25], [34]. The Lee code is configured to conduct the numerical experiments using the following standard parameters of this device [34]-[35]:

1. Bank parameters: Static inductance (L_0) = 36 nH, Bank capacitance (C_0) = 432 µF, and short-circuited resistance of the discharge circuit (r_0) = 1.2 mΩ.
2. Tube parameters: Cathode radius (b) = 15 cm, Anode radius (a) = 8 cm and Anode length (z_0) = 21.3 cm.
3. Operating parameters: Bank charging voltage (V_0) = 25 kV, Deuterium-Tritium (D-T) gas: (MW = 5, A =1 and At-1 mol-2 = 2) and Operating pressure (P_0) = appropriate range of pressure (Torr) in each gas.
4. Model parameters: Mass swept-up factor (f_m) = 0.0635 and plasma current factor (f_c) = 0.7 in the axial phase, Mass swept-up factor (f_{mr}) = 0.14 and plasma current factor (f_{cr}) = 0.7 in the radial phase.

These model parameters have been obtained by fitting the computed current trace with the measured one at 14.3 Torr D-T in KPU200 SPF [33]-[34]. Though, this set of model parameters is expected to vary slightly within a wide range of gases, even in a pressure range for a given gas [36]-[37] these are kept constant in our present numerical experiments for different gases in the pressure range of 0.1 – 19 Torr.

4 Results and Discussion

4.1 Ion beam Flux for Various Gases

The high-energy ions from plasma focus are applied for a different type of material processing. The operating pressure of Ar, Ne, and N_2 gases are varied and the corresponding flux, fluence, and energy of outgoing ion beam from pinch plasma in terms of I_{peak}, I_{pinch}, Z_{eff}, r_p, and U are obtained using the Eqs (1), (2), and (3) through the code. As an example, Table 1 presents the ion beam properties for Ar. This table shows that the peak discharge current (~1962 kA) at maximum pinch current (~773 kA) is found at 3.5 Torr whilst the Ar plasma goes to its 16th ionized state (Z_{eff} = 16) at 0.2 Torr. Also, I notice that the r_p gradually reduces with decreasing pressure up to 3.5 Torr and then gets its minimum value of 3.2 mm at 3.0 Torr. This reduced value remains unchanged up to 0.6 Torr after that it starts to increase again with pressure reduction.

Table 1 Change in ion beam properties with pressure variation of Ar plasma in KPU200 SPF.

P_0 (Torr)	I_{peak} (kA)	I_{pinch} (kA)	Z_{eff}	r_p ($\times 10^{-3}$ m)	U (kV)	Flux ($\times 10^{27}$ ions m^{-2} s^{-1})	Fluence ($\times 10^{20}$ ions.m^{-2})	E ($\times 10^4$ J)
10	1961.80	612.88	8.00	13.10	89.65	0.38	1.57	0.97
9	1943.30	650.79	8.00	11.55	98.20	0.56	2.15	1.13
8	1922.18	690.51	8.21	9.88	109.13	0.86	2.52	1.11
7	1897.70	720.48	8.48	8.53	122.66	1.22	3.28	1.25
6	1868.77	744.57	8.78	7.06	141.47	1.86	4.62	1.44
5	1833.65	762.26	9.10	5.55	170.97	3.03	6.82	1.65
4	1789.46	772.40	9.46	4.14	369.57	4.06	8.26	2.50
3.5	1762.43	772.99	9.66	3.53	558.07	4.71	8.93	3.03
3	1730.73	772.47	9.84	3.20	766.56	4.97	8.9	3.46
2.5	1692.62	766.59	9.91	3.20	661.90	5.25	8.78	2.97
2	1644.81	753.80	9.94	3.20	601.67	**5.31**	8.23	2.54
1.5	1578.03	731.04	9.94	3.20	678.63	4.71	6.43	2.24
1	1476.97	691.70	9.97	3.20	779.51	3.93	4.55	1.82
0.7	1384.71	653.73	10.39	3.20	629.59	3.82	3.97	1.34
0.2	1072.58	519.25	16.00	9.54	320.93	2.19	0.16	0.38
0.1	920.02	453.78	16.00	10.9	301.53	1.25	0.082	0.24

The diode voltage reaches its maximum value of 779.51 kV at 1.0 Torr. The flux curve of ions (m^{-2} s^{-1}) for Ar, Ne, and N_2 gases with pressure change is shown in Fig. 1.

The flux curve of Ar ions gradually increases with an increase in pressure to the maximum value of 5.31 × 1027 at 2 Torr and then reduces with further pressure increase.

The Ne curve has a value of 0.54 × 1027 at 1 Torr, rises sharply to a peak value of 4.78 × 1027 at 2.5 Torr, and then drops gradually. The N_2 curve shows the same trend with a lower peak flux value of 1.67 × 1027 at 4 Torr. During flux calculation, the pinch radii at the corresponding optimum pressure of Ar, Ne, and N_2 are found to be 3.2 mm, 4.69 mm, and 8.81 mm, respectively.

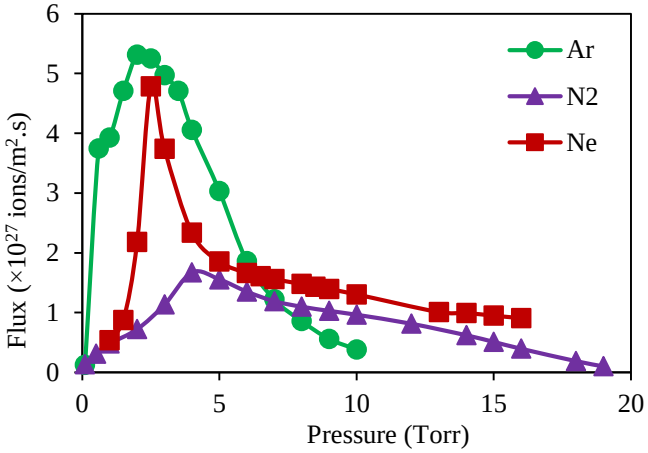

Fig. 1 Change in ion beam flux with pressure variation for Ar, Ne, and N_2 in KPU200 SPF.

This lowest value of pinch radii in Ar and Ne plasmas due to radiative collapse, produce the highest flux of ion beam compared to N_2 gas.

4.2 Ion Beam Fluence for Various Gases

The fluence in ions/m^2 for the various gases with pressure change is shown in Fig. 2. The curve shapes and the changing trend of fluence with pressure variation for various gases are comparable to the flux curves discussed in section 4.1. The peak values of the fluence are obtained as 8.93 ×1020 at 3.5 Torr Ar, 6.44 × 1020 at 2.5 Torr Ne, and 2.97 ×1020 at 4 Torr N_2. Noted, the optimum pressure and hence r_p for Ne and N_2 are similar to that for flux calculation.

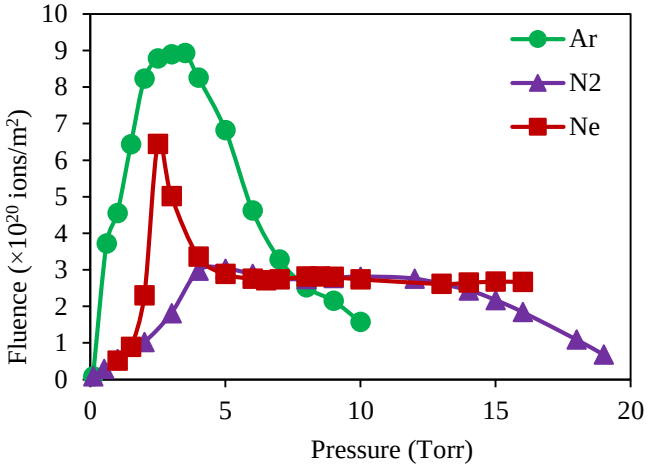

Fig. 2 Change in ion beam fluence with variation for Ar, Ne, and N_2 in KPU200 SPF.

At the optimum pressure, the pinch radius of Ar is found to be 3.53 mm which is quietly smaller than that of other gases. Also, the duration of the pinch (ion beam pulse duration) of Ar, Ne, and N_2 are computed as 190 ns, 144 ns, and 135 ns, respectively at their corresponding optimum pressure. Fluence is the flux multiplied by the estimated ion beam pulse duration. These two factors (the largest pulse duration and smallest pinch radius) enhance the fluence of Ar compared to Ne and N_2.

4.3 Ion Beam Energy for Various Gases

The ion beam energy rises with the increase in pressure until it reaches a high value and then reduces with further pressure increases as shown in Fig. 3.

In our present studies, the number of ions per shot and ion current along with ion beam energy is found in Ar plasma 2.86 ×

1016 and 252 kA with peak 3.46 × 104 J at 3 Torr, in Ne plasma 6.6 × 1016 and 430 kA with peak 1.83× 104 J at 8.5 Torr, and in N_2 plasma 9.14 × 1016 and 393 kA with peak 1.21 × 104 J at 6 Torr. Also, both of the Zeff and U(kV) are found as Ar(9.84 & 767), Ne(8 & 217), and N_2(5.74 & 144). That means the high atomic gases show a higher effective charge number and diode voltage than those of lighter gases. These are the reasons for greater ion beam energy for heavier gasses (reflection of Eq. (3)).

The computed results getting from the present study in KPU200 SPF are compared with those of NX2 [23] at similar pressures of Ar, Ne, and N_2 gases and are given in Table 2. The NX2 is a Mather type DPF device with operating energy of 2.7 kJ whilst its KPU200 SPF is 135 kJ. Due to this higher operating energy of this device, the I_{peak} and consequent I_{pinch} are almost 4-times higher for each of the gases. The variation trend of pinch properties such as z_p, r_p, V_{max}, Z_{eff}, and τ with gas are very similar in both devices.

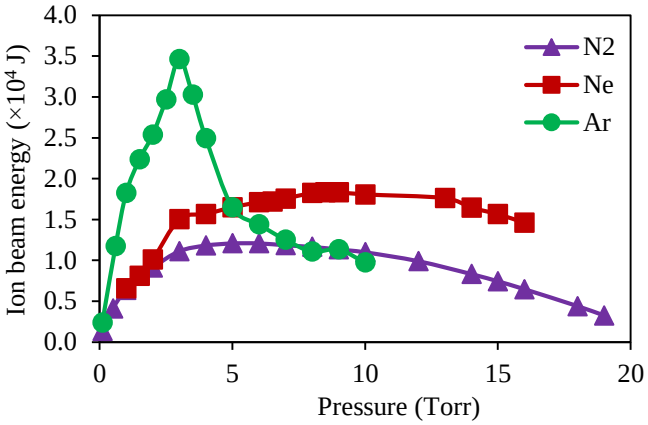

Fig. 3 Change in ion beam energy with variation for Ar, Ne, and N_2 in KPU200 SPF.

Table 2 Comparison of ion beam characteristics in NX2 [23] and KPU200 SPF.

DPF device	NX2	KPU200	NX2	KPU200	NX2	KPU200
Operating gas	Ar	Ar	Ne	Ne	N_2	N_2
P_0(Torr)	2	2	4	4	2	2
I_{peak}(kA)	406	1644.81	406	1644.76	395	1561.53
I_{pinch}(kA)	209	753.8	208	745.83	215	755.59
z_p(cm)	3.4	14.58	2.8	12.29	2.8	11.77
r_p(cm)	0.08	0.32	0.14	0.66	0.24	1.12
V_{max} (kV)	152	601.67	34	262.09	29	200.96
Z_{eff}	11	9.94	8	8	6.4	7
τ (ns)	30	154.87	25.2	144.07	25.6	141.48
Ion flux (×10^{27} ions/m^2 s)	14	**5.23**	6.6	**2.33**	3.2	**0.72**
Ion fluence (×10^{20} ions/m^2)	4.3	**8.23**	1.7	**3.36**	0.8	**1.02**
Ion beam energy (J)	207	**25400**	143	**15700**	13	**9100**

The obtained pinch radii in KPU200 SPF for different gases are very higher than those in NX2. According to Eq. (1), r_p has a strong effect (inversely proportional) on ion flux and this is because it in NX2 is higher than in the present SPF device for each gas whilst ion fluence is higher in KPU200 SPF because of its large pinch duration. The ion beam energy in this device is much higher due to its greater induced voltage than that of NX2. It is also observed that the variation trend of ion beam properties with change in pressure of these gases in both devices is very similar in nature. Finally, it is to be concluded that the obtained numerical results from my present studies are consistent that increasing the validation of this research work.

5 Conclusion

The electrode geometry of the spherical plasma focus device, KPU200 SPF has been obtained by applying the 'equivalent straightened electrode' technique to configure the Lee code. I use this code to characterize the ion beam flux (ions $m^{-2}s^{-1}$), fluence (ions/m^2), and energy (J) for Ar, Ne, and N_2 pinch plasmas with pressure variation in the DPF device. The computed results for each used gas indicate that all of these ion beam properties increase with the increase in pressure until reaching a peak value and then decrease with further pressure increase. The pinch radius of N_2 (8.81 mm) is about two times higher than that for Ar (3.2 mm) and Ne (4.69 mm). The lower values of pinch radii in Ar and Ne pinch plasmas cause radiative collapse and produce a higher ion beam flux in Ar(5.31 × 1027) and Ne(4.78 × 1027 at 2.5 Torr) than N_2 (1.67 × 1027 at 4 Torr). The pulse duration of Ar, Ne, and N_2 are found as 190 ns, 144 ns, and 135 ns, respectively, and the consequent peak fluences are found as 8.93 ×1020, 6.44 ×1020, and 2.97 ×1020, respectively. The Ar beam energy (3.46 × 104 J) is greater than Ne (0.83× 104 J) and N_2 (1.21 × 104 J) because of its higher values of the effective charge (9.84) and induced voltage (767 kV) generated by the collapse of pinch plasma.

The obtained results getting from this study in KPU200 SPF are compared with those of NX2 at similar pressures of Ar, Ne, and N_2. The variation trend of ion beam properties with change in pressure of these gases in both devices is very similar in nature which increases the validation of the results.

6 Acknowledgment

The author acknowledges the Physics discipline and Research cell, Khulna University for giving a sound environment and active support during this research work.

7 Conflict of Interest

The author declares that there is no conflict of interest regarding the publication of this article.

References

[1] Lee, S., Saw, S.H., Soto, L., Springham, S.V. and Moo, S.P., 2009. Numerical experiments on plasma focus neutron yield

versus pressure compared with laboratory experiments. *Plasma Physics and Controlled Fusion*, *51*(7), p.075006.

[2] Liu, M., 1996. *Soft X-rays from compact plasma focus* (Doctoral dissertation).

[3] Habibi, M., Amrollahi, R. and Etaati, G.R., 2010. Experimental study of hard X-ray emission with different anode tips in APF plasma focus device. *Journal of fusion energy*, *29*(1), pp.49-54.

[4] Filippov, N.V., Filippova, T.I. and Vinogradov, V.P., 1962. Dense high-temperature plasma in the region of non-cylindrical cumulation of Z-pinch. *Nucl. Fusion: Suppl*, p.577.

[5] Mather, J.W., 1964. Investigation of the high-energy acceleration mode in the coaxial gun. *The Physics of Fluids*, *7*(11), pp.S28-S34.

[6] Mather, J.W., 1965. Formation of a high-density deuterium plasma focus. *The Physics of Fluids*, *8*(2), pp.366-377.

[7] Saw, S.H., Damideh, V., Chong, P.L., Lee, P., Rawat, R.S. and Lee, S., 2014, August. A 160 kJ dual plasma focus (DuPF) for fusion-relevant materials testing and nano-materials fabrication. In *International Journal of Modern Physics: Conference Series* (Vol. 32, p. 1460322). The Authors.

[8] Hassan, M., Rawat, R.S., Lee, P., Hassan, S.M., Qayyum, A., Ahmad, R., Murtaza, G. and Zakaullah, M., 2008. Synthesis of nanocrystalline multiphase titanium oxycarbide (TiCxOy) thin films by UNU/ICTP and NX2 plasma focus devices. *Applied Physics A*, *90*(4), pp.669-677.

[9] Niranjan, R., Rout, R.K., Srivastava, R., Chakravarthy, Y., Mishra, P., Kaushik, T.C. and Gupta, S.C., 2015. Surface modifications of fusion reactor relevant materials on exposure to fusion grade plasma in plasma focus device. *Applied Surface Science*, *355*, pp.989-998.

[10] Ahmad, M., Al-Hawat, S. and Akel, M., 2013. Porous structure formation on silicon surface treated by plasma focus device. *Journal of Fusion Energy*, *32*(4), pp.471-478.

[11] Bhuyan, M., Mohanty, S.R., Rao, C.V.S., Rayjada, P.A. and Raole, P.M., 2013. Plasma focus assisted damage studies on tungsten. *Applied surface science*, *264*, pp.674-680.

[12] Niranjan, R., Rout, R.K., Tomar, B.S., Ramanjaneyulu, P.S., Paranjape, D.B. and Kaushik, T.C., 2018. Application of medium energy plasma focus device in study of radioisotopes. *Physics Letters A*, *382*(46), pp.3365-3368.

[13] Damideh, V., Chin, O.H., Saw, S.H., Lee, P.C.K., Rawat, R.S. and Lee, S., 2019. Characteristics of Fast ion beam in Neon and Argon filled plasma focus correlated with Lee Model Code. *Vacuum*, *169*, p.108916.

[14] Auluck, S., Kubes, P., Paduch, M., Sadowski, M.J., Krauz, V.I., Lee, S., Soto, L., Scholz, M., Miklaszewski, R., Schmidt, H. and Blagoev, A., 2021. Update on the scientific status of the plasma focus. *Plasma*, *4*(3), pp.450-669.

[15] Szydlowski, A., Banaszak, A., Bienkowska, B., Ivanova-Stanik, I.M., Scholz, M. and Sadowski, M.J., 2004. Measurements of fast ions and neutrons emitted from PF-1000 plasma focus device. *Vacuum*, *76*(2-3), pp.357-360.

[16] Akel, M., Salo, S.A., Saw, S.H. and Lee, S., 2014. Characterization of oxygen ion beams emitted from plasma focus. *Vacuum*, *110*, pp.54-57.

[17] Akel, M., Salo, S.A., Ismael, S., Saw, S.H. and Lee, S., 2017. Comparison of measured and computed beam ion current densities emitted from two 2 kJ plasma focus machines. *Vacuum*, *136*, pp.163-167.

[18] Lee, S., 2022. Radiative Dense Plasma Focus Computation Package: RADPF www.plasmafocus.net

[19] Lee, S., 2014. Plasma focus radiative model: Review of the Lee model code. *Journal of Fusion Energy*, *33*(4), pp.319-335.

[20] Lee, S. and Saw, S.H., 2017. The plasma focus—numerical experiments, insights and applications. In *Plasma Science and Technology for Emerging Economies* (pp. 113-232). Springer, Singapore.

[21] Scholz, M. and Ivanova-Stanik, I.M., 2000. Initial phase in plasma focus device—model and computer simulation. *Vacuum*, *58*(2-3), pp.287-293.

[22] Lee, S. and Saw, S.H., 2012. Plasma focus ion beam fluence and flux—Scaling with stored energy. *Physics of Plasmas*, *19*(11), p.112703.

[23] Lee, S. and Saw, S.H., 2013. Plasma focus ion beam fluence and flux—For various gases. *Physics of Plasmas*, *20*(6), p.062702.

[24] Maslov, V.V., Rumyantsev, V.G., Basmanov, V.F., Budnikov, D.V., Garin, A.V., Drozdov, I.Y., Ershov, D.A., Korkin, D.S., Makeev, N.G., Molodtsev, D.A. and Moskvin, N.I., 2014. A KPU-200 movable capacitor installation. *Instruments and Experimental Techniques*, *57*(2), pp.131-134.

[25] Zavyalov, N.V., Maslov, V.V., Rumyantsev, V.G., Drozdov, I.Y., Ershov, D.A., Korkin, D.S., Molodtsev, D.A., Smerdov, V.I., Falin, A.P. and Yukhimchuk, A.A., 2013. A source with a 1013 DT neutron yield on the basis of a spherical plasma focus chamber. *Plasma Physics Reports*, *39*(3), pp.243-247.

[26] Ay, Y., Al-Halim, M.A.A. and Bourham, M.A., 2016. MHD simulation for neutron yield, radiations and beam-ion properties in the spherical plasma focus. *Journal of Fusion Energy*, *35*(2), pp.407-414.

[27] Yaşar, A.Y., 2020. Neutron and Ion Production with Various Applied Voltages in Spherical Plasma Focus. *Dicle Üniversitesi Mühendislik Fakültesi Mühendislik Dergisi*, *11*(1), pp.135-141.

[28] Ay, Y., 2021. Spherical plasma focus operated with nitrogen and neon gases for soft x-rays (bremsstrahlung radiation, line radiation, and radiative recombination). *Plasma Physics and Controlled Fusion*, *63*(7), p.075011.

[29] Ay, Y., 2019. Effect of the cathode radius on plasma dynamics and radiation emissions in a spherical plasma focus device. *Physics of Plasmas*, *26*(10), p.102506.

[30] Ay, Y., 2021. Neon soft x-ray yield optimization in spherical plasma focus device. *Plasma Physics and Controlled Fusion*, *63*(11), p.115009.

[31] Lee, S., 2014. Radiative Dense Plasma Focus Computation Package: RADPF, 2010 http://www. plasmafocus. net. http://www. plasmafocus. net/IPFS/modelpackage/File1RADPF. htm. http://www. plasma focus. net/IPFS/modelpackage/File2Theory. pdf. http://www. plasma focus. net/IPFS/modelpackage. *UPF. htm*.

[32] Akel, M., Salo, S.A., Saw, S.H. and Lee, S., 2014. Properties of ion beams generated by nitrogen plasma focus. *Journal of Fusion Energy*, *33*(2), pp.189-197.

[33] Akel, M., Salo, S.A., Saw, S.H. and Lee, S., 2014. Ion beam features produced by two plasma focus machines operated with different gases. *IEEE Transactions on Plasma Science*, *42*(9), pp.2202-2206.

[34] Lee, S. and Saw, S.H., 2017. The plasma focus—numerical experiments, insights and applications. In *Plasma Science and Technology for Emerging Economies* (pp. 113-232). Springer, Singapore.

[35] Saw, S. H., 2012. Plasma focus numerical experiments and BORA—2370-6 school and training course on dense magnetized plasma as a source of ionizing radiations, their diagnostics and applications, *Abdus Salam International Centre for theoretical physics*, 8–12 Oct 2012.

[36] Akel, M., Ismael, S., Lee, S., Saw, S.H. and Kunze, H.J., 2017. Numerical experiments on the PF1000 plasma focus device operated with nitrogen and oxygen gases. *Modern Physics Letters B*, *31*(16), p.1750167.

[37] Lee, S., Saw, S.H. and Ali, J., 2013. Numerical experiments on radiative cooling and collapse in plasma focus operated in krypton. *Journal of Fusion Energy*, *32*(1), pp.42-49.